Journal of Industrial and Engineering Chemistry 32 (2015) 292–297

Contents lists available at ScienceDirect

Journal of Industrial and Engineering Chemistry

journal homepage: www.elsevier.com/locate/jiec

Epoxidation of propylene to propylene oxide with molecular oxygen over Sb_2O_3–CuO–NaCl/SiO_2 catalysts

Anusorn Seubsai [a,*], Daniel Noon [b], Thanaphat Chukeaw [a], Bahman Zohour [b], Waleeporn Donphai [a], Metta Chareonpanich [a], Selim Senkan [b]

[a] Department of Chemical Engineering, Faculty of Engineering, Kasetsart University, Bangkok 10900, Thailand
[b] Department of Chemical and Biomolecular Engineering, University of California Los Angeles, CA 90095, United States

ARTICLE INFO

Article history:
Received 9 June 2015
Received in revised form 16 August 2015
Accepted 24 August 2015
Available online 11 September 2015

Keywords:
Copper oxide
Antimony trioxide
Epoxidation
Propylene
Propylene oxide

ABSTRACT

Co-impregnated Sb_2O_3–CuO–NaCl/SiO_2 catalysts were investigated for the direct gas-phase synthesis of propylene oxide (PO) from propylene and molecular oxygen at atmospheric pressure. The trimetallic system was optimized for PO formation by varying the Sb:Cu:Na ratios, total metal loadings and calcination temperatures. At a reaction temperature of 250 °C and propylene/oxygen molar ratio = 1:4, the highest performing catalyst achieved 40–45% PO selectivity with 0.4–0.7% propylene conversion without a co-feeding gas. The coexistence of Sb_2O_3 and CuO crystals was determined to play a vital role in propylene epoxidation, while NaCl helped to suppress combustion.

Introduction

Propylene oxide (PO) is widely used in the preparation of various textiles and plastics [1,2]. Established industrial processes for its manufacture include the chlorohydrin and hydroperoxide routes. The former, however, produces chlorinated byproducts that pose environmental risks, while the latter requires the costly production or acquisition of H_2O_2 [3]. Hence, substantial efforts have been made to devise an alternate, scalable means of production. Arguably, the greatest potential lies in the direct gas-phase epoxidation of propylene to PO by molecular oxygen using heterogeneous catalysts. Nevertheless, research into this technique has proven to be challenging as the discovery of a high performing, economically viable catalyst continues to be elusive [3,4].

Over the past twenty years, some potentially promising catalytic materials have been studied. Ag-based catalysts, modified with various types of supports and co-catalysts [5–12], have not been used commercially since they facilitate the partial combustion of propylene, via the abstraction of the allylic hydrogen by adsorbed oxygen or the combustion of the allyl alkoxy intermediate [13]. Au-based catalysts have become attractive to several researchers because, in the presence of O_2 and H_2 under mild conditions (100–200 °C and 1 bar), they produce PO with excellent selectivities (>90%) [14–24]. But their propylene conversions are relatively low (1–9%) and, more problematically, the large amounts of H_2 required react with the gold and O_2 to generate hydroperoxy, which subsequently works as an oxidant [25,26].

More recently, Cu-based catalysts have become increasingly attractive for propylene epoxidation [7,27–39]. One study showed that a single crystal of metallic Cu was intrinsically more selective for the epoxidation of alkenes containing allylic hydrogen than Ag was [31]. And unlike Au-based catalysts, Cu-based ones require no H_2. On the other hand, the performance of Cu-based catalysts in the epoxidation of propylene has been limited, since partial combustion and acrolein formation fiercely compete with epoxidation [28,40], and so these catalysts struggle with low PO yield. PO selectivity has hardly exceeded 50% even at low propylene conversion (<20%). In attempts to improve PO yield, researchers have modified Cu catalysts with a variety of additional active metals, promoters and/or supports [7,27,32,33,35–37,41], with mixed results. The present work furthers that research.

Specifically, we investigated a recently discovered Cu-based trimetallic catalyst, Sb_2O_3–CuO–NaCl/SiO_2, that significantly enhances propylene epoxidation relative to catalysts comprised of the silica-supported metal oxides individually or in bimetallic form. The metal ratios, total metal loading on SiO_2 and calcination temperature were varied to optimize PO formation under atmospheric pressure and without a co-feeding gas. A time-on-stream evaluation was also performed to monitor the catalyst's stability and a regeneration method was also examined.

* Corresponding author. Tel.: +66 813786911; fax: +66 02 561 4621.
E-mail address: fengasn@ku.ac.th (A. Seubsai).

http://dx.doi.org/10.1016/j.jiec.2015.08.026
1226-086X/

Experimental

Catalyst preparation

All catalysts in this work were prepared by co-impregnation [27,33]. The unimetallic (Sb/SiO_2, Cu/SiO_2, $NaCl/SiO_2$), bi-metallic ($Sb–Cu/SiO_2$, $Sb–NaCl/SiO_2$, $Cu–NaCl/SiO_2$) and tri-metallic catalysts ($Sb–Cu–NaCl/SiO_2$) were prepared in parallel by mixing appropriate aqueous metal salt precursor solutions ($Cu(NO_3)_2.6H_2O$, $SbCl_3$, or NaCl; Alfa Aesar) with the SiO_2 support (Alfa Aesar, surface area of ~100 m^2/g). The solution volumes and support weights were varied to achieve catalysts comprising a comprehensive set of metal loadings. The mixtures were stirred at 20 °C for 24 h, allowing for the metal salts to diffuse into the support. This was followed by drying at 120 °C while mixing. The materials were subsequently air calcined at 460–540 °C for 6 h.

Activity test

Each catalyst (5 mg) was evaluated for performance at atmospheric pressure using a novel computer-controlled high-throughput array channel microreactor system capable of testing up to 80 catalysts in a single experiment [42]. The gas hourly space velocity (GSHV) was fixed at 20,000 h^{-1} using mass flow controllers (MKS, Andover, MA). The feed gas consisted of 1 vol% propylene (C_3H_6), 5 vol% O_2 and balance He at 250 °C for all experiments. Data analysis was conducted at a pseudo-steady condition (i.e. 2–4 h after the reactor reached 250 °C) [27,33] by an on-line Micro-Gas Chromatograph (GC, Varian, CP-4900) equipped with a thermal conductivity detector (TCD), Porapak U (10 m), and Molecular sieve 5 Å (10 m). The products PO, AC and CO_2 were consistently detected in substantial amounts, along with traces (<1%) of acetone (AT) and acetaldehyde (AD). The product selectivities and propylene conversions for each catalyst were calculated on the basis of carbon balance. PO selectivity (S_{PO}) and propylene conversion ($X_{C_3H_6}$) were calculated according to Eqs. (1) and (2), respectively:

$$\%S_{PO} = \frac{x_{PO}}{x_{PO} + x_{AC} + x_{AT} + (2x_{AD}/3) + (x_{CO_2}/3)} \cdot 100\% \quad (1)$$

$$\%X_{C_3H_6} = \frac{x_{PO} + x_{AC} + x_{AT} + (2x_{AD}/3) + (x_{CO_2}/3)}{x_{C_3H_6,\,feed}} \cdot 100\% \quad (2)$$

where each x denotes a corresponding species mole fraction in the reactor exit and $X_{C_3H_6,\,feed}$ is the feed C_3H_6 mole fraction. The repeatability of all experiments was within ±10%. In general, a variety of catalysts in the same set were prepared in parallel to minimize uncertainty. GC calibrations for gaseous species (propylene, O_2, CO_2) were conducted with He as the carrier gas, and calibrations for liquid species (PO, AC, AT, AD) were performed by vaporizing the injected liquids of these species in a heated, evacuated 2250 cm^3 stainless steel tank (He as carrier gas). Using peak area as the basis for GC calculations, all calibrations yielded linear five-point curves with $R^2 \geq 0.995$.

Catalyst characterization

N_2 physisorption, conducted with a Quantachrome Autosorp-1C instrument with BET and BJH methods at −196 °C, was used to measure the catalysts' specific surface area. Powder X-ray diffraction (XRD) patterns were obtained on an X-ray powder diffractometer (XRD: JEOL JDX-3530 and Philips X-Pert) using Cu Kα radiation, 45 kV and 40 mA to identify the active catalyst phase and average crystallite sizes. A scanning electron microscope and an energy dispersive X-ray spectrometer (SEM/EDS, SEM: JEOL, JSM-5410LV) operated at 20 keV were used to image the catalysts' morphology and elemental composition. Continuous H_2-temperature programmed reduction (H_2-TPR) measurements were carried out in a continuous-flow Inconel tube reactor held at 25–900 °C with a heating rate of 5 °C/min. The H_2/Ar mixture gas (9.6% H_2) was introduced into the catalyst bed at total flow rate of 30 cm^3/min. The H_2 consumption was continuously monitored by using a TCD-equipped GC (Shimadzu GC-2014). A Simultaneous TGA–DTA Analyzer (TA instrument, SDT2960 Simultaneous TGA–DTA Universal 2000) in air at a temperature range of 30–1000 °C was used to examine types of carbon on fresh and used catalysts.

Results and discussion

Fig. 1 shows an optimization of the Sb:Cu:Na metal ratio of the trimetallic system with the total metal loading fixed at 18 wt% for all catalysts. The results are plotted in the triangular diagrams in terms of PO selectivity (Fig. 1A) and propylene conversion (Fig. 1B). Each corner of the triangle represents the corresponding unimetallic Sb_2O_3/SiO_2, CuO/SiO_2 and $NaCl/SiO_2$ catalyst at 18 wt% loading. The bimetallic catalysts of $Sb_2O_3–CuO/SiO_2$, $Sb_2O_3–NaCl/SiO_2$ and $CuO–NaCl/SiO_2$ are on the perimeter of the triangle. Each

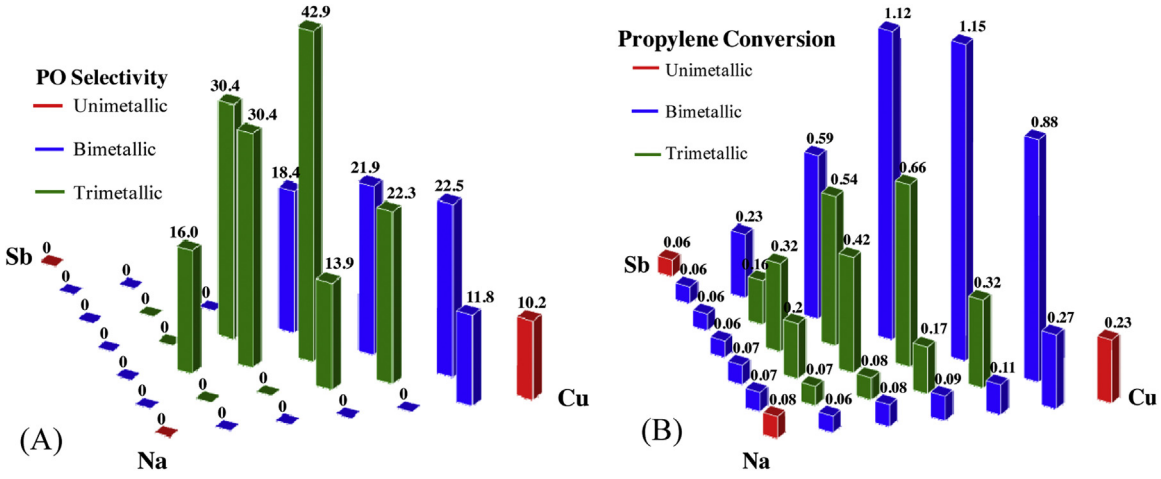

Fig. 1. Percent PO selectivities (A) and propylene conversions (B) as a function of Sb–Cu–Na concentrations on the SiO_2 support at 250 °C. All catalysts had a total metal loading of 18 wt% and were calcined at 500 °C.

step traversed on the perimeter entails a 3.0 wt% change in the loading of each metal on the bimetallic. All trimetallic Sb_2O_3–CuO–NaCl/SiO_2 catalysts are within the triangle's interior blocks. From Fig. 1, the trimetallic Sb_2O_3–CuO–NaCl/SiO_2 and bimetallic Sb_2O_3–CuO/SiO_2 catalysts exhibit remarkably superior PO selectivities (up to 42%) and propylene conversions (up to 1.15%) compared to the unimetallic Sb_2O_3/SiO_2 and NaCl/SiO_2 and bimetallic catalysts Sb_2O_3–NaCl/SiO_2 and most of the CuO–NaCl/SiO_2 combinations (Cu:Na = 12:6, 9:9, 6:12, and 3:15 by weight), which exhibit virtually 0% PO selectivity. The unimetallic CuO/SiO_2 catalyst achieves 10.2% PO selectivity with 0.23% propylene conversion. Doping CuO/SiO_2 with a small amount of NaCl (Cu:Na = 15:3 by weight) has a promotional effect, giving 11.8% PO selectivity at 0.27% propylene conversion, consistent with earlier works done by Lambert et al. [28]. Clearly, the combined presence of Sb_2O_3, CuO and NaCl enables synergistic effects for propylene epoxidation catalysis.

The catalyst comprising a weight (molar) ratio for Sb:Cu:Na of 2:3:1 (1.0:2.9:2.6) was the most productive for epoxidation, with selectivities for PO, AC and CO_2 at 43%, 6% and 51%, respectively at a propylene conversion of 0.66%. Interestingly, when comparing the optimum ratio to the proximate bimetallic Sb_2O_3–CuO ratios (e.g. Sb:Cu = 12:6 and 9:9), the PO selectivity of the trimetallic catalyst was about twice that of the bimetallics, but the propylene conversion was about half. This indicates that the coexistence of Sb_2O_3 and CuO in the catalyst plays an important role in propylene epoxidation and that NaCl acts as a promoter for the reaction [43,44]. It is important to note that highly active sites of other catalysts for propylene epoxidation (e.g. Ag catalysts [6], RuO_2/SiO_2 [33]) generally create a route for combustion [45]. The addition of NaCl can, therefore, reduce the reactivity of the catalyst surface for propylene combustion and thereby improve the PO selectivity but reduce propylene conversion [45,46]. This is because NaCl crystals are incorporated into the catalyst's solid structure and so primarily occupy the highly active sites on the catalyst surface responsible for combustion of propylene or intermediates. After NaCl captures the highly active sites for propylene combustion, the route for PO generation becomes more pronounced and the PO selectivity is increased. Since the overall combustion (i.e. CO_2 formation) is partially inhibited by addition of NaCl, the propylene conversion is expected to be reduced as confirmed here [47].

In an attempt to further optimize the performance of the Sb_2O_3–CuO–NaCl/SiO_2 catalysts for PO synthesis, an investigation of the effects of total metal loading from 3 to 20 wt% on the SiO_2 support was undertaken. The results of catalytic performance are shown in Fig. 2, and the XRD spectra of selected catalysts (5, 9, 13, 18 and 20 wt%) are presented in Fig. 3. Note that the selectivities of other byproducts (such as AT and AD) are insignificant compared

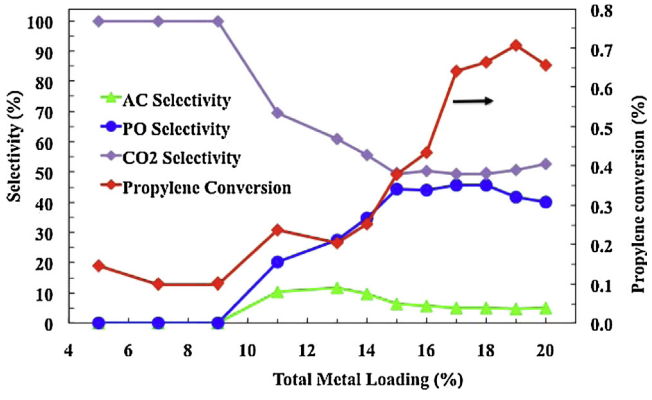

Fig. 2. Effect of total metal loading on SiO_2 from 3 to 20 wt%, Sb:Cu:Na = 2:3:1. The catalysts were calcined at 500 °C.

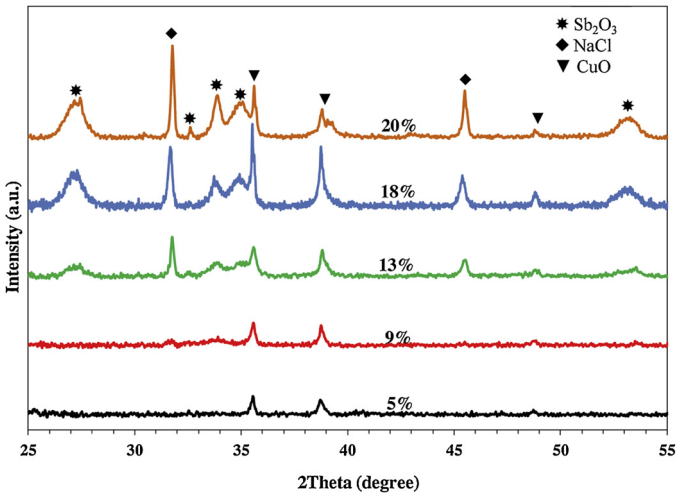

Fig. 3. XRD spectra of 5, 9, 13, 18 and 20 wt% total metal loading on SiO_2, Sb:Cu:Na = 2:3:1. The catalysts were calcined at 500 °C.

to CO_2, PO and AC. At low total metal loadings (5, 7 and 9 wt%), only CO_2 was detected. The XRD spectrum at 9 wt% suggests CuO is the only crystalline species, i.e. Sb_2O_3 and NaCl are either amorphous or constituted crystals too small to be detected ($\lesssim$2.0 nm). When further increasing the loading from 9 to 15 wt%, the PO selectivity rapidly increased from 0 to a maximum of about 45%, while the propylene conversion increased from 0.10 to 0.40%. At 13 wt%, XRD suggests the presence of Sb_2O_3 and NaCl crystals, in addition to the previously detected CuO, potentially accounting for the sudden rise in PO production. Also, at higher loadings, crystals of Sb_2O_3 and CuO are more likely to be adjacent, allowing for synergistic catalysis toward PO. Below 13 wt%, CuO and Sb_2O_3 crystals may be more isolated from each other for this to occur; therefore, these materials function in the manner of the unimetallic CuO/SiO_2 catalyst, which generally produces significant amounts of AC [33].

In between 15 and 18 wt%, the PO selectivity is constant at ~45% as well as AC selectivity at ~5%, whereas the propylene conversion rises sharply from 0.40 to 0.66%. Beyond this loading, the aforementioned synergistic catalysis deteriorates, leading to a rise in CO_2 selectivity. The propylene conversion, however, continues to increase, simply because the number of active Sb_2O_3–CuO–NaCl phases (i.e. the proximity of Sb_2O_3 and CuO crystals) increased. Fig. 3 indicates that the average Sb_2O_3 crystallite size according to the Sherrer equation at 20 wt% (23 nm) is larger than that of 18 wt% (21 nm), implying the sintering of active Sb_2O_3 that reduces the PO selectivity and propylene conversion for loadings above the optimal PO yield at 18 wt% (44% PO selectivity, 0.66% propylene conversion). This implies that when the crystallite size becomes larger, the agglomerates of crystallites also tend to become larger such that the overall contact area between Sb_2O_3 and CuO crystals, responsible for the synergistic catalysis, lessens.

The metal distributions (Sb, Cu and Na) of the catalysts prepared at different total metal loading were also investigated by SEM/EDS. The images are shown in Fig. 4. Each metal was uniformly dispersed on the SiO_2 support.

Fig. 5 shows the relationship between PO formation and calcination temperature. The catalysts were calcined at 460, 480, 500, 520 and 540 °C for 6 h. The propylene conversion was the highest for the catalyst calcined at 460 °C, but CO_2 was the main product. The propylene conversion decreased with increasing PO selectivity until achieving the optimum PO selectivity at 500 °C, i.e. the same calcination temperature used for preparing the catalysts in Figs. 1 and 2. Temperatures >500 °C resulted in decreased PO

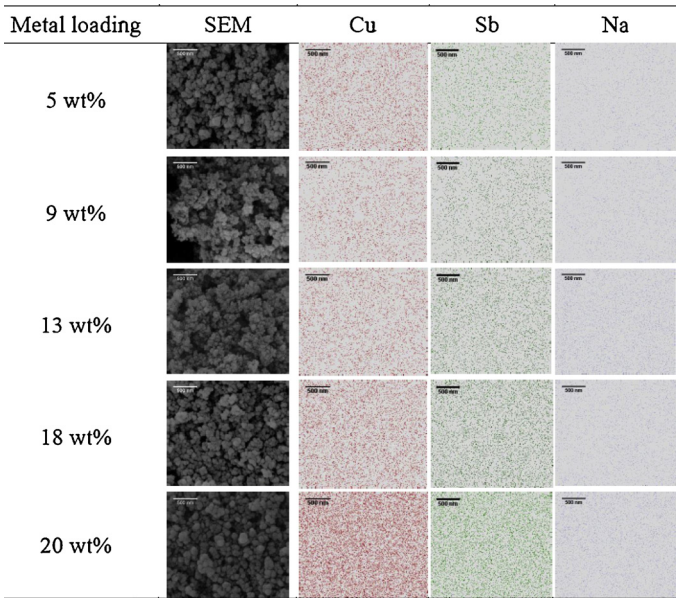

Fig. 4. SEM/EDS of catalysts at 5, 9, 13, 18 and 20 wt% total metal loading on SiO_2, Sb:Cu:Na = 2:3:1. The catalysts were calcined at 500 °C. Each scale bar is 500 nm.

formation. The AC selectivity was virtually fixed at about 5% until dropping precipitously at 540 °C.

The XRD spectra of the catalysts examined in Fig. 5 are presented in Fig. 6, and the BET surface area versus the crystallite sizes of Sb_2O_3, CuO and NaCl is shown in Fig. 7. The analyses of the XRD spectra reveal the characteristic diffraction patterns of Sb_2O_3 (2θ = 27.3, 32.5, 33.8, 34.8, 53.2°), CuO (2θ = 35.6, 38.7, 48.9°) and NaCl (2θ = 31.7, 45.5°). At all calcination temperatures, the crystallinity and the crystallite size of NaCl were virtually unchanged at ~100 nm according to the Sherrer equation. Above 480 °C, the crystallite sizes of CuO remain about the same (at 76–79 nm) but the intensity of the characteristic CuO peaks slightly increased, indicating that the quantity of CuO crystals slightly increased with rising the calcination temperatures.

The most significant influence on PO formation is the crystallite Sb_2O_3 size. The XRD spectra of Sb_2O_3 are broader at lower calcination temperatures, indicating smaller crystallite sizes. The crystallite Sb_2O_3 size is 14, 19, 21, 23 and 24 nm at 460, 480, 500, 520 and 540 °C, respectively. Considering that the propylene conversion decreases with increasing calcination temperature (see Fig. 5), the increase in crystallite size with increasing calcination

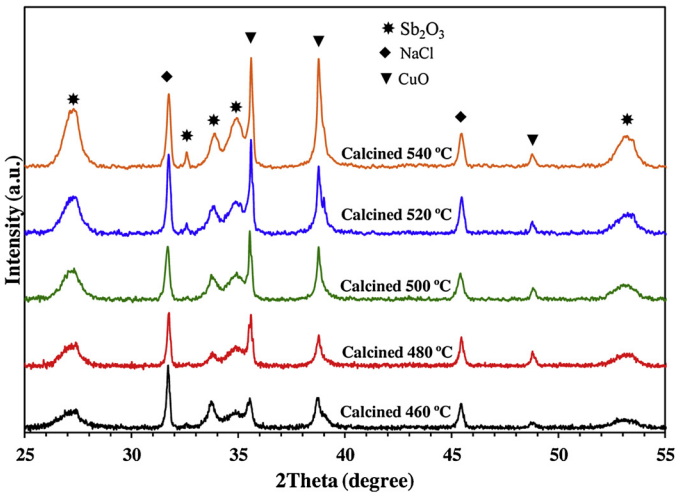

Fig. 6. XRD spectra of Sb_2O_3–CuO–NaCl/SiO_2 catalysts calcined at 460–540 °C.

temperature is consistent with a reduction of active surface area as indicated in Fig. 7. The optimum PO selectivity occurs at 500 °C. Below 500 °C, the decrease in PO production rate with increasing calcination temperature is smaller than the decrease in CO_2 production rate. Above 500 °C however, the larger crystallite Sb_2O_3 sizes (i.e. the fewer active sites) apparently have a stronger influence on the reduction of PO formation than on the reduction of CO_2 formation. These results suggest that both the presence and sizes of Sb_2O_3, CuO and NaCl crystals play a significant role in PO formation.

H_2-TPR measurements, shown in Fig. 8, were conducted to examine the interaction between the distinct Sb_2O_3 and CuO phases in the Sb_2O_3–CuO–NaCl/SiO_2 catalyst at 18% total metal loading and calcined at 500 °C. The unimetallic CuO/SiO_2 and Sb_2O_3/SiO_2 catalyst showed a single peak around 300 and 570 °C, attributed to the reduction of bulk CuO [48] and Sb_2O_3 [49], respectively. The bimetallic Sb_2O_3–CuO/SiO_2 catalyst showed two peaks, a main peak at 300 °C and a shoulder around 390 °C. The peak at the lower temperature is attributed to the reduction of CuO, and the shoulder at higher temperature is ascribed to the reduction of Sb_2O_3. The presence of CuO, presumably in close proximity or completely contact with Sb_2O_3, appears to shift the Sb_2O_3 peak to lower temperatures. Therefore, in the bimetallic of Fig. 8, Sb_2O_3 and CuO are reduced almost simultaneously because of a spillover induced by the reduction of CuO [50]. Similarly, the

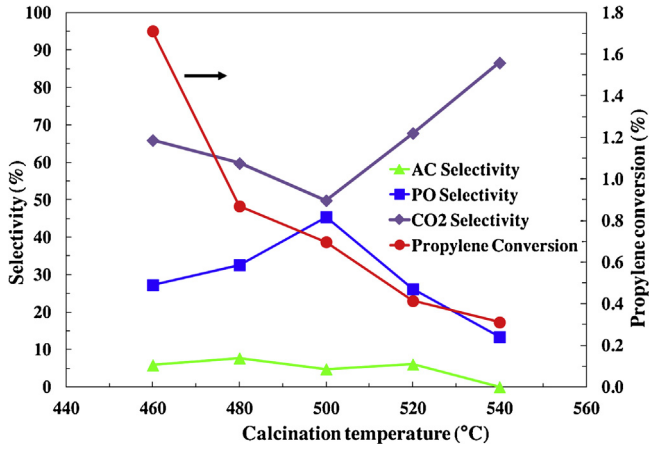

Fig. 5. Catalytic activity of the Sb_2O_3–CuO–Na/SiO_2 (Sb:Cu:Na = 2:3:1, 18 wt%) catalyst calcined at different temperatures.

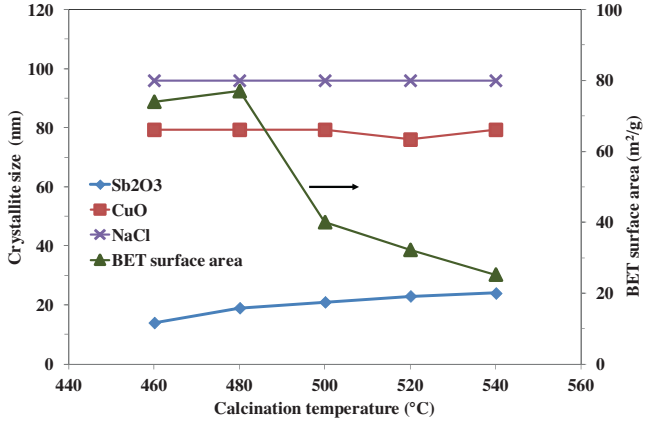

Fig. 7. Crystallite sizes of Sb_2O_3, CuO and NaCl; and BET surface area of the Sb_2O_3–CuO–Na/SiO_2 (Sb:Cu:Na = 2:3:1, 18 wt%) catalyst calcined at 460–540 °C.

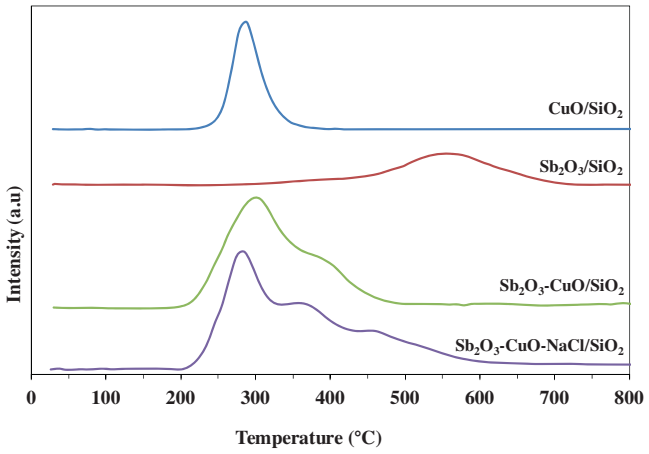

Fig. 8. H_2-TPR profiles of Sb_2O_3, CuO, CuO–Sb_2O_3 and CuO–Sb_2O_3–NaCl on SiO_2. For each metal indicated, the loading is 6, 9 and 3 wt% for Sb, Cu and Na, respectively.

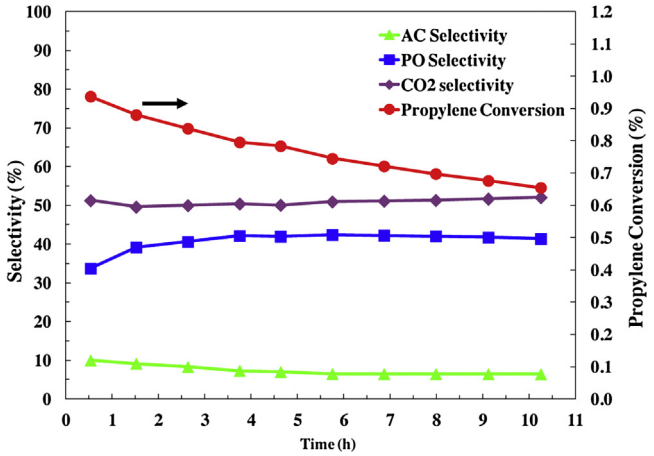

Fig. 9. Time-on-stream testing results Sb_2O_3–CuO–NaCl/SiO_2 catalysts; Sb:Cu:Na = 2:3:1 at 18 wt% total metal loading and calcined at 500 °C.

trimetallic Sb_2O_3–CuO–NaCl/SiO_2 catalyst shows the main reduction peak of CuO around 300 °C and two shoulders around 370 and 460 °C. The 370 °C shoulder is attributed to the Sb_2O_3 phases that are in close proximity to CuO phases, while that at 460 °C is assigned to Sb_2O_3 phases displaced from CuO phases. The addition of NaCl may separate some of the Sb_2O_3 phases by blocking the contact of the two metal oxides [51]. These H_2-TPR results corroborate the notion that the Sb_2O_3 and CuO phases are in close proximity, and thus may enhance the synergistic effects of the catalysts for the title reaction.

Since the addition of NaCl induces both the apparent phase separation of Sb_2O_3 from CuO while improving the catalyst's performance, the active sites of the Sb_2O_3–CuO/SiO_2 bimetallic essentially have a surplus of Sb_2O_3 that attenuates PO formation and enhances combustion. Hence, NaCl may favorably assist in finely tuning the localized spatial metal oxide composition on the surface of the catalyst support.

Since catalyst durability is essential, a time-on-stream test of the Sb_2O_3–CuO–Na/SiO_2 catalyst with the optimal composition (i.e. Sb:Cu:Na = 2:3:1 at 18 wt% total metal loading on SiO_2 and calcined at 500 °C) for propylene epoxidation using oxygen was performed. Fig. 9 charts PO and AC selectivities together with propylene conversions over 10 h of continuous operation at 250 °C. The XRD (Fig. 10A), TGA–DTA (Fig. 10B) and BET surface area measurements of the fresh and used catalyst were carried out to investigate its deactivation. As indicated in Fig. 9, PO selectivity gradually increased during the first 3 h, reaching a maximum of about 42%. During hours 3–10, PO selectivity minimally decreased to 41%, while propylene conversion continuously decreased from 0.95% at the first hour to 0.65% at 10 h. Evidently, this is due to the coalescence of crystals (i.e. catalyst sintering). As is indicated in Fig. 10A, the crystallite size of Sb_2O_3 particles increased during the experiment – 21 nm on the fresh catalyst compared to 23 nm on the used catalyst. This increase in crystallite size is consistent with BET surface area analysis; the surface area of the catalyst after 10 h of reaction was found to be 35 m^2/g compared to 40 m^2/g of the fresh catalyst. The reduction in the Sb_2O_3 crystallite surface area accordingly weakens the synergy between Sb_2O_3 and CuO responsible for PO formation. TGA–DTA analyses (shown in Fig. 10B) showed no coke formation. The TGA and TDA curves of the fresh and used catalysts were virtually unchanged, suggesting no carbonaceous compounds were generated and then deposited on the catalyst. Both the fresh and used catalysts exhibited weight loss around 600–800 °C; this could be due to the changing oxide states of CuO or Sb_2O_3.

After the 10 h of performance testing, the catalyst was stirred in 1.0 M HCl for 24 h in an effort to regenerate it. The material was then dried at 120 °C and calcined at 500 °C for 6 h. This procedure was found to elevate the PO selectivity to 40% (53% CO_2 selectivity and 7% AC selectivity at 0.84% propylene conversion) at 1.5 h of a time-on-stream evaluation, similar to the results of the fresh catalyst shown in Fig. 9. Also, the XRD spectrum of this material was identical to that of the fresh catalyst (in Fig. 10A). The dilute solution of HCl dissolves CuO and Sb_2O_3, enabling the re-calcination step to recover the original crystallite morphology and thus catalytic performance characteristics.

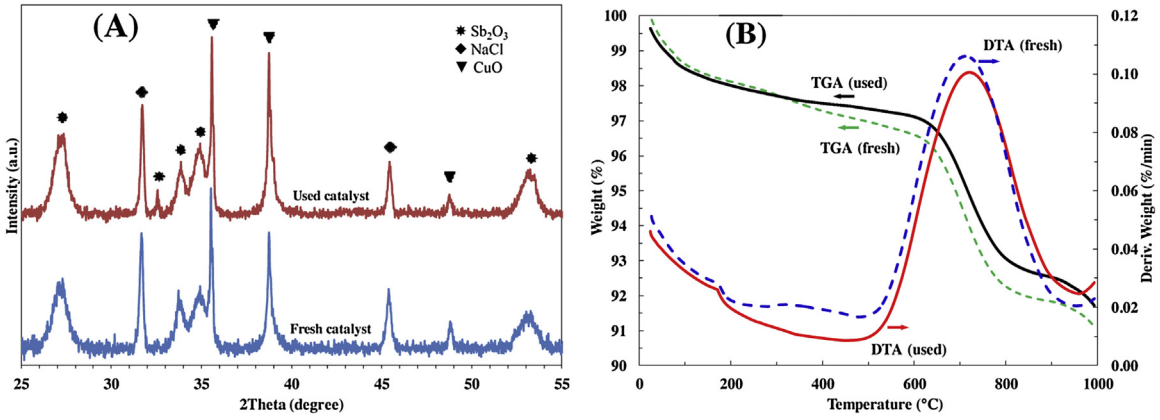

Fig. 10. (A) XRD patterns and (B) TGA–DTA curves of fresh and used Sb_2O_3–CuO–NaCl/SiO_2 catalyst; Sb:Cu:Na = 2:3:1 at 18 wt% total metal loading and calcined at 500 °C.

Conclusion

Co-impregnated catalysts of Sb_2O_3–CuO–NaCl/SiO_2 were studied by first maximizing the catalytic performance for propylene epoxidation with respect to the metal ratios of Sb:Cu:Na with the total metal loading and calcination temperature of fixed at 18 wt% and 500 °C. Peak performance (43% with 0.66% propylene conversion) occurred at Sb:Cu:Na = 2:3:1 by weight. Since the 18 wt% total metal loading maximized the PO yield, it was chosen to explore the effects of calcination temperature between 480 and 540 °C. The coexistence of the crystallinity of Sb_2O_3 and CuO was found to be essential in the epoxidation, and NaCl acted as a promoter, enhancing PO selectivity by reducing combustion. The stability of the trimetallic catalyst was tested continuously over a 10-h period; the catalyst exhibited a slow deactivation due to sintering. However, it can be regenerated by dissolving in dilute HCl and re-calcining.

Acknowledgement

A. Seubsai acknowledges the Kasetsart University Research and Development Institute (KURDI), the Thailand Research Fund (TRF) and the Commission on Higher Education (TRG5780257) for financial support. B. Zohour and D. Noon acknowledge Chemical and Bimolecular Engineering Department at UCLA for financial support.

References

[1] D. Kahlich, U. Wiechern, J. Lindner, Propylene Oxide, Ullmann's Encyclopedia of Industrial Chemistry, John Wiley & Sons, Inc, 2000p. 1.
[2] Y. Miao, G. Lu, X. Liu, Y. Guo, Y. Wang, Y. Guo, J. Ind. Eng. Chem. 16 (2010) 45.
[3] T.A. Nijhuis, M. Makkee, J.A. Moulijn, B.M. Weckhuysen, Ind. Eng. Chem. Res. 45 (2006) 3447.
[4] F. Cavani, J.H. Teles, ChemSusChem 2 (2009) 508.
[5] J.R. Monnier, Appl. Catal. A 221 (2001) 73.
[6] J.Q. Lu, M.F. Luo, H. Lei, C. Li, Appl. Catal. A 237 (2002) 11.
[7] J.Q. Lu, M.F. Luo, H. Lei, X.H. Bao, C. Li, J. Catal. 211 (2002) 552.
[8] A. Takahashi, N. Hamakawa, I. Nakamura, T. Fujitani, Appl. Catal. A 294 (2005) 34.
[9] D. Sullivan, P. Hooks, M. Mier, J.W. van Hal, X.K. Zhang, Top. Catal. 38 (2006) 303.
[10] W. Yao, Y. Guo, X. Liu, Y. Guo, Y. Wang, Y. Wang, Z. Zhang, G. Lu, Catal. Lett. 119 (2007) 185.
[11] G. Jin, G. Lu, Y. Guo, Y. Guo, J. Wang, X. Liu, Catal. Today 93–95 (2004) 173.
[12] Y. Lei, F. Mehmood, S. Lee, J. Greeley, B. Lee, S. Seifert, R.E. Winans, J.W. Elam, R.J. Meyer, P.C. Redfern, D. Teschner, R. Schlogl, M.J. Pellin, L.A. Curtiss, S. Vajda, Science 328 (2010) 224.
[13] E.A. Carter, W.A. Goddard, J. Catal. 112 (1988) 80.
[14] T. Hayashi, K. Tanaka, M. Haruta, J. Catal. 178 (1998) 566.
[15] B.S. Uphade, S. Tsubota, T. Hayashi, M. Haruta, Chem. Lett. (1998) 1277.
[16] B.S. Uphade, T. Akita, T. Nakamura, M. Haruta, J. Catal. 209 (2002) 331.
[17] M. Haruta, M. Date, Appl. Catal. A 222 (2001) 427.
[18] A.K. Sinha, S. Seelan, S. Tsubota, M. Haruta, Angew. Chem. Int. Ed. 43 (2004) 1546.
[19] B. Chowdhitry, J.J. Bravo-Suarez, M. Date, S. Tsubota, M. Haruta, Angew. Chem. Int. Ed. 45 (2006) 412.
[20] J. Chen, S.J.A. Halin, E.A. Pidko, M.W.G.M. Verhoeven, D.M.P. Ferrandez, E.J.M. Hensen, J.C. Schouten, T.A. Nijhuis, ChemCatChem 5 (2013) 467.
[21] W.S. Lee, M. Cem Akatay, E.A. Stach, F.H. Ribeiro, W. Nicholas Delgass, J. Catal. 287 (2012) 178.
[22] W.S. Lee, M. Cem Akatay, E.A. Stach, F.H. Ribeiro, W. Nicholas Delgass, J. Catal. 308 (2013) 98.
[23] J. Huang, T. Takei, T. Akita, H. Ohashi, M. Haruta, Appl. Catal. B 95 (2010) 430.
[24] J. Huang, E. Lima, T. Akita, A. Guzmán, C. Qi, T. Takei, M. Haruta, J. Catal. 278 (2011) 8.
[25] E.E. Stangland, K.B. Stavens, R.P. Andres, W.N. Delgass, J. Catal. 191 (2000) 332.
[26] C. Sivadinarayana, T.V. Choudhary, L.L. Daemen, J. Eckert, D.W. Goodman, J. Am. Chem. Soc. 126 (2004) 38.
[27] A. Miller, B. Zohour, A. Seubsai, D. Noon, S. Senkan, Ind. Eng. Chem. Res. 52 (2013) 9551.
[28] O.P.H. Vaughan, G. Kyriakou, N. Macleod, M. Tikhov, R.M. Lambert, J. Catal. 236 (2005) 401.
[29] W.M. Zhu, Q.H. Zhang, Y. Wang, J. Phys. Chem. C 112 (2008) 7731.
[30] Y. Wang, H. Chu, W.M. Zhu, Q.H. Zhang, Catal. Today 131 (2008) 496.
[31] R.M. Lambert, F.J. Williams, R.L. Cropley, A. Palermo, J. Mol. Catal. A: Chem. 228 (2005) 27.
[32] J. He, Q. Zhai, Q. Zhang, W. Deng, Y. Wang, J. Catal. 299 (2013) 53.
[33] A. Seubsai, M. Kahn, S. Senkan, ChemCatChem 3 (2011) 174.
[34] M. Kahn, A. Seubsai, I. Onal, S. Senkan, Top. Catal. 53 (2010) 86.
[35] W.G. Su, S.G. Wang, P.L. Ying, Z.C. Feng, C. Li, J. Catal. 268 (2009) 165.
[36] X. Zheng, Q. Zhang, Y. Guo, W. Zhan, Y. Guo, Y. Wang, G. Lu, J. Mol. Catal. A: Chem. 357 (2012) 106.
[37] S. Kalyoncu, D. Duzenli, I. Onal, A. Seubsai, D. Noon, S. Senkan, Z. Say, E. Vovk, E. Ozensoy, Catal. Lett. 145 (2015) 596.
[38] D. Duzenli, E. Seker, S. Senkan, I. Onal, Catal. Lett. 142 (2012) 1234.
[39] X. Yang, S. Kattel, K. Xiong, K. Mudiyanselage, S. Rykov, S.D. Senanayake, J.A. Rodriguez, P. Liu, D.J. Stacchiola, J.G. Chen, Angew. Chem. Int. Ed. 54 (2015) 1.
[40] H. Tuysuz, J.L. Galilea, F. Schuth, Catal. Lett. 131 (2009) 49.
[41] A. Seubsai, M. Kahn, B. Zohour, D. Noon, M. Charoenpanich, S. Senkan, Ind. Eng. Chem. Res. 54 (2015) 2638.
[42] S. Senkan, K. Krantz, S. Ozturk, V. Zengin, I. Onal, Angew. Chem. Int. Ed. 38 (1999) 2794.
[43] A. Seubsai, B. Zohour, D. Noon, S. Senkan, ChemCatChem 6 (2014) 1215.
[44] S. Kalyoncu, D. Duzenli, I. Onal, A. Seubsai, D. Noon, S. Senkan, Catal. Commun. 61 (2015) 16.
[45] D. Torres, N. Lopez, F. Illas, R.M. Lambert, Angew. Chem. Int. Ed. 46 (2007) 2055.
[46] J. Lu, J.J. Bravo-Suárez, M. Haruta, S.T. Oyama, Appl. Catal. A 302 (2006) 283.
[47] A. Seubsai, S. Senkan, ChemCatChem 3 (2011) 1751.
[48] T. Nanba, S. Masukawa, J. Uchisawa, A. Obuchi, J. Therm. Anal. Calorim. 113 (2013) 793.
[49] S.A. D'Ippolito, M.A. Banares, J.L.G. Fierro, C.L. Pieck, Catal. Lett. 122 (2008) 252.
[50] R. Prins, Chem. Rev. 112 (2012) 2714.
[51] V.A. Mazzieri, C.L. Pieck, C.R. Vera, J.C. Yori, J.M. Grau, Appl. Catal. A 353 (2009) 93.